

Collective excitations of trapped Bose condensates in the energy and time domains

Dermot McPeake,^{*} Halvor Møll Nilsen,[†] and J F McCann
*Department of Applied Mathematics and Theoretical Physics,
 Queen's University Belfast, Belfast BT7 1NN, Northern Ireland and
 Institute of Physics, University of Bergen, Allégaten 55, N-5007 Bergen, Norway*
 (Dated: November 2001)

A time-dependent method for calculating the collective excitation frequencies and densities of a trapped, inhomogeneous Bose-Einstein condensate with circulation is presented. The results are compared with time-independent solutions of the Bogoliubov-deGennes equations. The method is based on time-dependent linear-response theory combined with spectral analysis of moments of the excitation modes of interest. The technique is straightforward to apply, is extremely efficient in our implementation with parallel FFT methods, and produces highly accurate results. The method is suitable for general trap geometries, condensate flows and condensates permeated with vortex structures.

PACS numbers: PACS numbers: 42.50.Hz, 32.80.Bx, 32.80.Rm

I. INTRODUCTION

The equations defining the frequencies of single particle excitations from a weakly-interacting dilute Bose gas at zero temperature were introduced by Bogoliubov [1] and applied to low-temperature Fermi systems by de Gennes [2]. The underlying assumption is that temperatures are sufficiently low such that the condensate is not significantly depleted and that the interparticle interactions are weak and the gas dilute. Under such constraints the dynamics are dominated by single particle excitations meaning that semiclassical approximations can be used for the field excitations and the equations are equivalent to linear response theory [3, 4, 5]. Trapped hydrostatic ultracold gas clouds can be modeled to a high degree of precision under these conditions. Even within this framework the equations must be solved numerically because of the inhomogeneity and nonlinearity of the condensate. Determining the elementary excitations is much more complex in situations in which the condensate is flowing or permeated with defects such as vortex arrays. The extraordinary coldness of the atom cloud means the condensate dynamics occur on millisecond time scales and thus are accessible to measurement as they evolve. Shape distortions, created by manipulating the condensate with external electromagnetic fields, can be used to measure mode frequencies [6, 7, 8], wave-mixing [9] and damping rates [10]. In this way elementary excitation frequencies at low temperatures can be measured to an accuracy within a few percent, and the agreement with theory for the low-lying modes is astonishingly good [5]. Precise measurements closer to the critical temperature are much more uncertain, and indeed theoretical modeling is also challenged by the influence of complex pair excitations

[11]. The agreement between theory and experiment is much less satisfactory in this region.

The experimental and theoretical study of condensates in the time domain mirrors experimental breakthroughs in ultrashort laser pulses used to probe ultrafast processes in chemistry and biology. Dynamic simulations and experiments applied to Bose condensates have provided insight into the transition from superfluid flow to dissipation and drag [12, 13] and in condensate formation and destruction. Trapped condensates are particularly suited to spectral methods, specifically the split-operator technique [14] combined with the FFT method [15]. We report results in which efficient parallel computing techniques have been implemented within the spectral method to determine the elementary excitation frequencies and densities. The method is ideally suited to the analysis of elementary excitations in complex flows and in the presence of defects. The method also allows the excitation mechanism of experiments to be modeled realistically and thus help devise schemes which produce optimal excitation of certain modes or superposition of modes leading to squeezed and entangled states [17], and observe collective excitations of quadrupoles giving evidence of superfluid motion [18, 19].

The paper is structured as follows: In section II the units and notation are described, and the field equations are introduced. The case of excitation in the presence of condensate circulation is discussed. The equations describing excitations in a cylindrically symmetric trap and quadrupole excitations in an asymmetric trap are given. In section III the time-dependent method is formulated. Finally, in sections IV and V, results are compared between the two methods and some general conclusions are given on the relative merits of each method.

^{*}Electronic address: d.mcpeake@am.qub.ac.uk

[†]Electronic address: halvor.nilsen@fi.uib.no

Interaction Strength C	Chemical potential (μ)	
	$\kappa = 0$	$\kappa = 1$
0	1.000000	2.000000
10	1.620434	2.368791
50	3.020229	3.489876
100	4.143006	4.513850
250	6.415956	6.685521
500	9.003106	9.213175
1000	12.678320	12.840724

TABLE I: Values of the chemical potential (μ) of the $\kappa = 0$ and $\kappa = 1$ states for the isotropic 2D trap as a function of interaction strength, C , in units of $\hbar\omega_0$

C	$\kappa = 0$		$\kappa = 1$	
	TDLR	DVR	TDLR	DVR
0	1.9995	2.0000	1.9996	2.0000
50	1.9998	2.0000	1.9998	2.0000
100	1.9936	2.0000	1.9979	2.0000
250	1.9977	2.0000	1.9980	2.0000
500	1.9978	2.0000	1.9978	2.0000
1000	1.9978	2.0000	1.9977	2.0000

TABLE II: Comparison of TDLR and DVR results for the excitation frequencies ω_j , for the mode $q_r = 1, q_\theta = 0$ with $\kappa = 0, 1$.

II. TIME-INDEPENDENT QUANTIZED FIELD EQUATIONS

The dilute system of N bosonic atoms mass m is trapped by external fields $V_{\text{ext}}(\mathbf{r})$ and interacts weakly through the two-body $V(\mathbf{r}, \mathbf{r}')$. If the external field is the static trapping potential, the Hamiltonian for the system can be written

$$\hat{H}' = \int d\mathbf{r} \hat{\Psi}^\dagger(\mathbf{r}) H_0 \hat{\Psi}(\mathbf{r}) + \frac{1}{2} \iint d\mathbf{r} d\mathbf{r}' \hat{\Psi}^\dagger(\mathbf{r}) \hat{\Psi}^\dagger(\mathbf{r}') V(\mathbf{r}, \mathbf{r}') \hat{\Psi}(\mathbf{r}') \hat{\Psi}(\mathbf{r}) \quad (1)$$

with $H_0 = -\frac{\hbar^2}{2m}\nabla^2 + V_{\text{trap}}(\mathbf{r}) - \mu$, with chemical potential μ . The interactions can be represented perturbatively by the pseudopotential $V(\mathbf{r}, \mathbf{r}') = U_0\delta(\mathbf{r} - \mathbf{r}')$ where the interaction is proportional to the s -wave scattering length a , $U_0 = 4\pi\hbar^2 a/m$. Bogoliubov's approximation, valid at

C	TDLR	DVR
0	2.0000	2.0000
50	1.5569	1.5569
100	1.5003	1.5002
250	1.4561	1.4561
500	1.4380	1.4380
1000	1.4277	1.4276
∞	1.4142	1.4142

TABLE III: Comparison of TDLR and DVR results for the quadrupole excitation $q_r = 0, q_\theta = \pm 2$ mode with condensate $\kappa = 0$.

C	$q_\theta = -2$		$q_\theta = 2$	
	TDLR	DVR	TDLR	DVR
0	0.0000	0.0000	2.0000	2.0000
50	0.8333	0.8331	1.8647	1.8649
100	1.0299	1.0300	1.7752	1.7748
250	1.1876	1.1871	1.6590	1.6594
500	1.2565	1.2560	1.5902	1.5906
1000	1.3027	1.3022	1.5388	1.5393

TABLE IV: Comparison of TDLR and DVR results for quadrupole excitation $q_r = 0, q_\theta = \pm 2$ for a condensate with circulation $\kappa = 1$.

low temperatures, treats the condensate semiclassically while quantizing the excitations so that:

$$\hat{\Psi}(\mathbf{r}) = \sqrt{N} \phi(\mathbf{r}) + \hat{\psi}(\mathbf{r}) \quad (2)$$

The condensate wavefunction satisfies the Gross-Pitaevskii equation:

$$H_0(\mathbf{r})\phi(\mathbf{r}) + NU_0|\phi(\mathbf{r})|^2\phi(\mathbf{r}) = 0 \quad (3)$$

Then expanding $\hat{\psi}$ in modes

$$\hat{\psi}(\mathbf{r}) = \sum_j \left[u_j(\mathbf{r})\hat{\alpha}_j + v_j^*(\mathbf{r})\hat{\alpha}_j^\dagger \right] \quad (4)$$

The eigenvalue problem reduces to the Bogoliubov-deGennes equations in the form:

$$\mathcal{L}u_j(\mathbf{r}) + NU_0\phi^2v_j(\mathbf{r}) = \hbar\omega_ju_j(\mathbf{r}) \quad (5a)$$

$$\mathcal{L}v_j(\mathbf{r}) + NU_0\phi^{*2}u_j(\mathbf{r}) = -\hbar\omega_jv_j(\mathbf{r}) \quad (5b)$$

where $\mathcal{L} = H_0(\mathbf{r}) + 2NU_0|\phi(\mathbf{r})|^2$. Time-reversal symmetry is reflected in the fact that every set of solutions $\{E_j, u_j, v_j\}$ has a corresponding set $\{-E_j, u_j^*, v_j^*\}$. For $E_j > 0$ the functions u_j, v_j are orthogonal with normalization

$$\int d\mathbf{r} (|u_j(\mathbf{r})|^2 - |v_j(\mathbf{r})|^2) = 1 \quad (6)$$

In our model the trap is represented by an asymmetric harmonic well:

$$V_{\text{trap}}(\mathbf{r}) = \frac{1}{2}m\omega_0^2(e_x^2x^2 + e_y^2y^2 + e_z^2z^2)$$

where $e_{x,y,z}$ are restoring force strengths, and ω_0 the natural angular frequency. Numerical calculations are carried out in scaled dimensionless units. Length, time and energy are given in units: $(\hbar/2m\omega_0)^{\frac{1}{2}}$, ω_0^{-1} and $\hbar\omega_0$, respectively.

When particle interactions are weak, corresponding to the ideal gas limit, the energies for an asymmetric trap are given by the oscillator formula

$$E_n = (n_x + \frac{1}{2})e_x + (n_y + \frac{1}{2})e_y + (n_z + \frac{1}{2})e_z$$

with $n_x, n_y, n_z = 0, 1, 2, \dots$. For a 2D symmetric oscillator ($e_z = 0, e_x = e_y = 1$) the cylindrical quantum numbers (q_r, q_θ) can be used:

$$E_n = n_x + n_y + 1 = 2q_r + |q_\theta| + 1$$

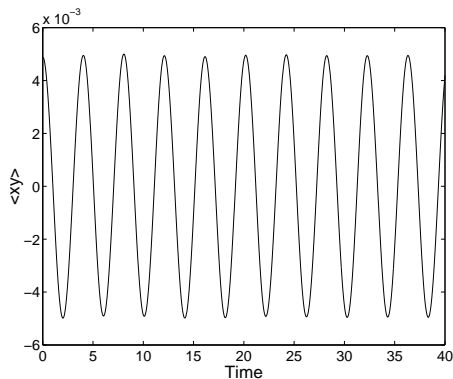


FIG. 1: Quadrupole moment evolution $f_{xy}(t)$ for low-lying excitations of a condensate with $\kappa = 0$.

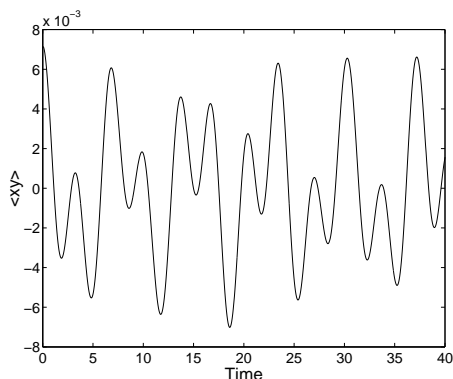


FIG. 2: Quadrupole moment evolution $f_{xy}(t)$ for low-lying excitations of a condensate with $\kappa = 1$. The figure displays interference between the modes $q_\theta = \pm 2$

with $q_r = 0, 1, 2, \dots$ and $q_\theta = 0, \pm 1, \pm 2, \dots$ so that the excitation frequencies above the ground state ($q_r = 0, q_\theta = \kappa$) are: $\omega_j = 2q_r + |q_\theta + \kappa| - \kappa$.

A. Excitations of vortex states

A precise test is provided by low-dimensional models for which highly accurate results can be obtained. It also allows the study of excitations in the presence of vortices. For a single vortex line with circulation κ along the axis of a cylindrically symmetric trap $e_x = e_y = 1, e_z = 0$:

$$\phi(r, \theta) = \tilde{\phi}(r)e^{i\kappa\theta} \quad (7)$$

$$\begin{aligned} -\left(\frac{\partial^2}{\partial r^2} + \frac{1}{r}\frac{\partial}{\partial r} - \frac{\kappa^2}{r^2}\right)\tilde{\phi}(r) + \frac{1}{4}r^2\tilde{\phi}(r) \\ + C|\tilde{\phi}|^2\tilde{\phi}(r) = \mu\tilde{\phi}(r) \end{aligned} \quad (8)$$

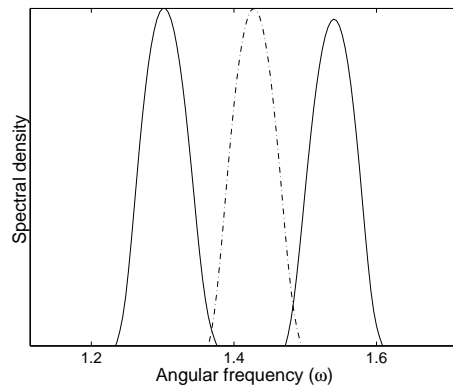


FIG. 3: Power spectral density of quadrupole moments $\langle xy \rangle$ versus angular frequency. The vertical scale is logarithmic and ranges from 0.1 to 1.0. Results for $\kappa = 0$, dashed line, $q_\theta = \pm 2$ and $\kappa = 1$, solid lines, $q_\theta = \pm 2$ for interaction strength $C = 1000$.

where $C = 8\pi a N_a$ with N_a the linear density of atoms in the \hat{z} direction. The excitations can be written:

$$\begin{aligned} u_j(r, \theta) &= \tilde{u}_{q_r}(r)e^{i(q_\theta + \kappa)\theta} \\ v_j(r, \theta) &= \tilde{v}_{q_r}(r)e^{i(q_\theta - \kappa)\theta} \end{aligned} \quad (9)$$

where $j = \{q_r, q_\theta\}$. The eigensystem equations (5a,5b) become

$$\begin{aligned} \left[-\frac{\partial^2}{\partial r^2} - \frac{1}{r}\frac{\partial}{\partial r} + \frac{(q_\theta + \kappa)^2}{r^2} + \frac{1}{4}r^2 - \mu + 2C|\tilde{\phi}|^2\right]\tilde{u}_{q_r}(r) \\ + C\tilde{\phi}^2\tilde{v}_{q_r}(r) = \omega_{q_r}\tilde{u}_{q_r}(r) \end{aligned} \quad (10)$$

$$\begin{aligned} \left[-\frac{\partial^2}{\partial r^2} - \frac{1}{r}\frac{\partial}{\partial r} + \frac{(q_\theta - \kappa)^2}{r^2} + \frac{1}{4}r^2 - \mu + 2C|\tilde{\phi}|^2\right]\tilde{v}_{q_r}(r) \\ + C\tilde{\phi}^2\tilde{u}_{q_r}(r) = -\omega_{q_r}\tilde{v}_{q_r}(r) \end{aligned} \quad (11)$$

B. Discrete variable representation

Equations (8),(10) and (11) are solved using the discrete variable representation (DVR) [20]. The condensate and excitation functions are represented by a Lagrange mesh $\tilde{\phi}, \tilde{u}_{q_r}, \tilde{v}_{q_r}$.

$$\tilde{\phi}(\mathbf{r}) = \sum_{i=1}^N \tilde{\phi}(r_i)f_i(r) \quad (12)$$

$$\tilde{u}_{q_r}(\mathbf{r}) = \sum_{i=1}^N \tilde{u}_{q_r}(r_i)f_i(r) \quad (13)$$

$$\tilde{v}_{q_r}(\mathbf{r}) = \sum_{i=1}^N \tilde{v}_{q_r}(r_i)f_i(r) \quad (14)$$

where $f_i(r)$ are Lagrange interpolating functions constructed from a set of orthonormal functions

$$\chi_k(r) = h_k^{-\frac{1}{2}} w(r)^{\frac{1}{2}} p_k(r) \quad (15)$$

such that

$$f_i(r) = \sum_{k=0}^{N-1} \chi_k^*(r_i) \chi_k(r) \quad (16)$$

We employ generalized Laguerre polynomials [21] $p_k(r) = L_k^\alpha(r) = ((\alpha + k)!/k!\alpha!) {}_1F_1(-k; \alpha + 1; r)$ associated with the weight function $w(r) = r^\alpha e^{-r}$ and normalization factor $h_k = (k + \alpha)!/k!$. The representation of the centrifugal energy terms of equations (10),(11) can be marginally improved by using different values of α [20]. Different grids for each angular momentum state requires the use of interpolation to connect different states for $\kappa \neq 0$. However using a common grid is more practical. The DVR results presented correspond to $k = N = 50$ and the common value $\alpha = 1$ so that:

$$f_i(r) = \frac{1}{\chi_N'(r_i)} \frac{\chi_N(r)}{r - r_i} \quad (17)$$

where the mesh points r_i are the N zeros of $L_N^\alpha(r)$. Applied to the coupled equations (8),(10),(11) this method reduces the problem to that of solving a system of nonlinear equations for the condensate and a linear eigenvalue problem for the excitations. The set of $(N + 1)$ nonlinear equations is efficiently solved using Newton's method where μ is an unknown and normalization of $\tilde{\phi}$ is imposed. As the functions $\tilde{\phi}, \tilde{u}, \tilde{v}$ are to be represented on the same grid points, r_i , an adequate coverage of points is required. A scaling factor h [20] is used to contract the natural mesh so that it extends to $\sim 1.5r_{\text{TF}}$ where $r_{\text{TF}} \approx 2(C/2\pi)^{1/4}$ is the Thomas-Fermi radius. Increasing the number of mesh points beyond $N = 50$ does not improve the accuracy beyond the figures quoted. While the matrices are dense they give results far more accurate than finite difference methods using similar sized matrices. We used a standard library routine for solution of the eigenvalue problem [24].

III. TIME-DEPENDENT LINEAR RESPONSE EQUATIONS

The mean-field approximation to the field operator is $\psi(\mathbf{r}, t) \approx \langle \Psi(\mathbf{r}, t) \rangle \approx \langle \Psi^\dagger(\mathbf{r}, t) \rangle$. The angular brackets denote averaging with respect to highly-occupied ($N \gg 1$) condensate number states. The evolution equation for the mean field is the time-dependent Gross-Pitaevskii equation [3]:

$$i\hbar \frac{\partial}{\partial t} \psi(\mathbf{r}, t) = \left[-\frac{\hbar^2}{2m} \nabla^2 + V_{\text{ext}}(\mathbf{r}, t) + NU_0 |\psi(\mathbf{r}, t)|^2 \right] \psi(\mathbf{r}, t) \quad (18)$$

The external potential includes the trapping potential and a small time-dependent perturbation: $V_{\text{ext}}(\mathbf{r}, t) = V_{\text{trap}}(\mathbf{r}) + V_{\text{pert}}(\mathbf{r}, t)$. The system responds to this perturbation by populating modes selected by the symmetry of the perturbation:

$$\psi(\mathbf{r}, t) \approx e^{-i\mu t} \phi(\mathbf{r}) + \sum_j [a_j(t) u_j(\mathbf{r}) e^{-i\omega_j t - i\mu t} + b_j(t) v_j(\mathbf{r}) e^{i\omega_j t - i\mu t}] \quad (19)$$

The oscillations of the system provides data for the frequencies: ω_j . This replaces the nonlinear coupled equation eigenvalue problem by an initial value problem followed by spectral analysis. Alternatively, we can introduce a perturbed initial state $\Psi(\mathbf{r}, 0)$ seeded with the spatial form to overlap with the symmetry of the desired excited state. This is equivalent to a sudden perturbation of the system. To study low-energy excitations the ground state, $\phi(\mathbf{r})$, is found by propagation of equation (18) in imaginary time [13] using a trial wavefunction. Implementing the split-operator FFT method on a parallel computer using between 1 and 16 processors. The method is extremely well-suited for nonlinear evolution equations [14]. In imaginary time the highly-excited modes are exponentially suppressed, and while it is not necessary to eliminate these modes before introducing the perturbation, a pure ground state is more efficient for spectral analysis.

The dipole modes were excited by a sudden but small displacement of the trap center. The subsequent center-of-mass oscillations are known exactly ($\omega = e_x, e_y, e_z$) and should provide precise benchmarks for the numerical method employed. Breathing (monopole) modes were excited selectively, and in line with experimental methods [6], by adjusting the force constants to compress or expand the condensate $e_{x,y} \rightarrow 1 \pm \varepsilon$. The low-lying quadrupole modes are accessible by seeding the initial state with a term of the appropriate symmetry. For example, adjusting the true ground state to $\Psi(\mathbf{r}, 0) = \phi(\mathbf{r})(1 + \varepsilon xy)$, and following the evolution of $\Psi(\mathbf{r}, t)$ under the Gross-Pitaevskii equation, the beats of the xy quadrupole spectrum are evident. While single modes may be selected by adiabatic perturbations of selected frequencies, sudden and strong perturbations can be used to gain data on higher excited modes. A significant advantage of the method is that a variety of perturbations of *different* symmetries can be used simultaneously to obtain the excitations by a *single* evolution of the nonlinear equations.

The wave packet method combined with spectral method was pioneered by Feit and Fleck [15] and has been used widely [16, 22, 23]. The response of the system is measured by the moment:

$$f_A(t) = \int d\mathbf{r} \Psi^*(\mathbf{r}, t) A(\mathbf{r}) \Psi(\mathbf{r}, t) \quad (20)$$

The excitation frequencies emerge from the Fourier transform of $f_A(t)$. The finite sampling time means that the

power spectral density signal can be improved by windowing. The windowing function we use is a β -valued Kaiser function chosen to minimize the background. The local maximum of the power spectrum is then used to identify the frequencies. The density profiles of the quasi-particles can be extracted by further spectral analysis. Once the appropriate ω_j is known the Fourier transform: $g_j^\pm(\mathbf{r}) = T^{-1} \int_0^T e^{i(\mu \pm \omega_j)t} \Psi(\mathbf{r}, t) dt$ isolates the corresponding amplitude. For both the imaginary time and real time propagation we used the same split-operator scheme. In the calculations we used a grid of 64 points in each dimension. To create the ground state we used a variable time step along with extrapolation to increase the speed of calculation and control the accuracy of the ground state. To obtain an accurate spectral resolution a total propagation time of ~ 30 times the trap period is necessary. In addition, the signal was processed with a windowing mask. Alternatively if the perturbation is small and introduced slowly, on the timescale of several trap periods, only a very small number of modes will be excited. The correlation $f_A(t)$ can be fitted to a Fourier expansion in just a few frequencies. This has been done for all the frequencies presented in this paper and gives equivalent accuracy while requiring only 3 trap periods.

A. Classical limit

When interparticle forces dominate the quantum pressure ($C \rightarrow \infty$) and the hydrodynamic limit is reached. The equilibrium condensate density, $\rho \equiv |\psi|^2$, for $\kappa = 0$ corresponds to the Thomas-Fermi distribution:

$$\rho_0(\mathbf{r}) = (\mu - V(\mathbf{r})) / C \quad (21)$$

Acoustic modes of excitation [25] $\rho(\mathbf{r}, t) = \rho_0(\mathbf{r}) + \rho'(\mathbf{r}) e^{-i\omega t}$ are determined by the equation [26]

$$\omega^2 \rho' = -2C \nabla \cdot (\rho_0 \nabla \rho') \quad (22)$$

For the 2D cylindrical trap ($e_x = e_y = 1, e_z = 0$) this gives ($C \rightarrow \infty$):

$$\omega_c^2 = 2q_r(q_r + 1) + q_\theta(2q_r + 1). \quad (23)$$

where the radial and angular quantum numbers (q_r, q_θ) are as defined above.

For a 3D asymmetric trap ($e_x \neq e_y \neq e_z$) the lowest quadrupole modes of scissors motion [18, 19, 26] that is of the form $\rho' \propto xy, yz, xz$ are given by the solutions: $\omega_{xy}^2 = e_x^2 + e_y^2$, $\omega_{yz}^2 = e_y^2 + e_z^2$, and $\omega_{zx}^2 = e_z^2 + e_x^2$.

IV. RESULTS

In this article we compare the time-dependent (TDLR) and time-independent methods (DVR) for excitation in 2D traps. For the DVR calculations we used $N = 30$ and $N = 50$ radial mesh points with a scaling factor

C	ω_{xy}	ω_{xz}	ω_{yz}
0	3.0005	4.0003	5.0002
10	2.8059	3.8041	4.7938
50	2.5439	3.5536	4.4612
100	2.4432	3.4228	4.2521
250	2.3521	3.3134	4.0254
500	2.3101	3.2609	3.8951
1000	2.2821	3.2257	3.7993
∞	2.2361	3.1623	3.6056

TABLE V: Lowest-energy quadrupole modes for an asymmetric trap with $e_x = 1, e_y = 2$ and $e_z = 3$ as a function of interaction strength C . Results for $C = \infty$ correspond to the hydrodynamic limit (23)

$h = 0.08$. The results presented, using $N = 50$, are converged to at least 6 decimal places. For reference, the values of the chemical potential are presented in Table I. The TDLR calculations were performed on grids of $64 \times 64 \times 64$ points. Convergence and accuracy can be calibrated by comparison with exact results. For example, the 2D dipole ($q_r = 0, q_\theta = 1$) mode is a feature of the trap and independent of the particle interactions (C) and circulation κ , so that $\omega_j = 1$. The DVR results for this mode are accurate to at least six decimal places, while the TDLR results are within 0.3% of the exact values over the range $0 \leq C \leq 1000$. Table II shows the results for the lowest breathing mode ($q_r = 1, q_\theta = 0$) for $\kappa = 0$ and $\kappa = 1$. Again, in 2D this mode is not sensitive to particle interactions. TDLR results are stable and consistent for this mode as C increases, slightly underestimating the frequency in the fourth significant figure. The loss of precision in the TDLR results for high C is of the same order as the errors in the chemical potential results.

The quadrupole modes are more sensitive to changes in C and also to the condensate circulation. In figure 1 the correlation $f_{xy}(t)$ is shown for $C = 1000$. The smooth sinusoidal curve translates to the Fourier transform spectral density shown as the dashed line in figure 3. The spectral density shows a noise-free profile with a well-defined peak at the value $\omega = 1.4277$. As $C \rightarrow +\infty$, $\omega \rightarrow \sqrt{2}$. In Table III results are presented for the mode: $\kappa = 0, q_r = 0, q_\theta = \pm 2$. The agreement between the time-dependent and time independent results is extremely good over the entire range of C . Given that the dipole mode showed the TDLR accuracy is within four figures, the accord to five figures for $C = 250$ and $C = 500$ is fortuitous.

When condensate circulation is present the quadrupole circulation can flow with or against the background and the $q_\theta = \pm 2$ modes split. This is evident in the beats arising in the $f_{xy}(t)$ correlation figure 2 and the corresponding spectrum (figure 3). The agreement with DVR results, indicated in Table IV is excellent. Since the TDLR method is based upon a cartesian grid, it is readily used for arbitrary geometries of the trap. For example, the quadrupole modes xy, yz, zx of an asymmetric 3D ellip-

soidal trap can found in the same way. In this case we used a mixed perturbation of all three symmetries and then frequency analyzed the correlations of each moment. The results are presented in Table V. The data tends to the correct high C limit uniformly and accurately.

V. CONCLUSION

We have compared methods for calculation of the excitation frequencies of a condensate at zero temperature. The method based on linear response theory is extremely efficient and successful at producing accurate results and

can be tailored to the experimental methods used to create the excitations of interest. The method is straightforward to implement, yields reliable results, and can be computed cheaply and efficiently. The versatility of the method extends to complex trap geometries and condensate topologies. Thus it is suitable for the study of excitations and sound propagation in traps where the condensate contains soliton and vortex structures [27].

We are very grateful for the support of Bergen Computational Physics Laboratory in the framework of the European Community - Access to Research Infrastructure action of the Improving Human Potential Programme.

-
- [1] N. Bogoliubov, *Izv. Akad. Nauk. SSSR* **11**, 77 (1947).
 [2] P. G. de Gennes *Superconductivity of Metals and Alloys*, (Benjamin, New York, 1966).
 [3] D. Pines And P. Nozières, *Theory of Quantum Liquids: Vol. II* (Addison-Wesley, Redwood City, Calif., 1960).
 [4] M. Edwards, P. A. Ruprecht, K. Burnett, R. J. Dodd and C. W. Clark C. W., *Phys. Rev. Lett.* **77**, 1671 (1996).
 [5] F. Dalfovo, S. Giorgini, L. P. Pitevsikii and S. Stringari, *Rev. Mod. Phys.* **71**, 463 (1999).
 [6] D. S. Jin, J. R. Enscher, M. R. Matthews, C. E. Wieman and E. A. Cornell, *Phys. Rev. Lett.* **77**, 420 (1996).
 [7] D. M. Stamper-Kurn, M. R. Andrews, A. P. Chikkatur, S. Inouye, H.-J. Miesner, J. Stenger and W. Ketterle, *Phys. Rev. Lett.* **80**, 2027 (1998).
 [8] M. R. Andrews, D. M. Kurn, H.-J. Miesner, D. S. Durfee, C. G. Townsend, S. Inouye and W. Ketterle, *Phys. Rev. Lett* **79** 553 (1997).
 [9] L. Deng, E.W. Hagley, J. Wen, M. Trippenbach, Y. Band, P. S. Julienne, J. E. Simsarian, K. Helmerson, S. L. Rolston and W. D. Phillips *Nature* **398**, 218 (1999).
 [10] O. Marago, G. Hechenblaikner, E. Hodby and C. Foot, *Phys. Rev. Lett.* **86** 3938 (2001).
 [11] D. A. W. Hutchinson, R. J. Dodd, and K. Burnett, *Phys. Rev. Lett.* **81**, 2198 (1998).
 [12] C. Raman, M. Köhl, R. Onofrio, D. S. Durfee, C. E. Kuklewicz, Z. Hadzibabic and W. Ketterle, *Phys. Rev. Lett.* **83**, 2502 (1999).
 [13] T. Winiecki, B. Jackson, J. F. McCann and C. S. Adams, *J. Phys. B: At. Mol. Opt. Phys.* **19**, 4069 (2000).
 [14] T. R. Taha and M. J. Ablowitz, *J. Comp. Phys.* **55**, 203 (1984).
 [15] M. D. Feit, J. A. Fleck, Jr. and A. Steiger, *J. Comp. Phys.* **47**, 412 (1982).
 [16] R. Kosloff, *J. Phys. Chem.* **92**, 2087 (1988).
 [17] C. Orzel, A.K. Tuchman, M. L. Fenselau, M. Yasuda and M. A. Kasevich, *Science* **291**, 2386 (2001).
 [18] D. Guéry-Odelin and S. Stringari, *Phys. Rev. Let.* **83**, 4452 (1999).
 [19] O. M. Maragò, S. A. Hopkins, J. Arlt, E. Hodby, G. Hechenblaikner and C. J. Foot, C. J., *Phys. Rev. Lett.* **84**, 2056-9 (2000).
 [20] D. Baye and P.-H. Heenan, *J. Phys. A*, **19**, 2041, (1986).
 [21] M. A. Abramowitz and I. E. Stegun *Handbook of Mathematical Functions and Tables* (Dover, New York, 1965).
 [22] J. C. Light, I. P. Hamilton and J. V. Lill, *J. Chem. Phys.* **82**, 1400 (1985).
 [23] V. A. Ermoshin and A. K. Kazansky, *Phys. Lett. A*, **218**, 99 (1996).
 [24] NAG library eigenvalue solver for a dense matrix: version 19 **f02ecf**
 [25] E. M. Lifschitz and L. Pitaevskii, *Statistical Physics: Part 2* (Pergamon, New York, 1980)
 [26] S. Stringari, *Phys. Rev. Lett* **77**, 2360 (1996).
 [27] J. R. Abo-Shaer, C. Raman, J. M. Vogels, W. Ketterle, *Science* **292**, 476 (2001).